1 3/351 JH

Geometric, thermal, and temporal constraints on the development of extensional faults at Bare Mountain (Nevada) and implications for neotectonics of the Yucca Mountain region

David A. Ferrill Center for Nuclear Waste Regulatory Analyses, 6220 Culebra Road, San Antonio, Texas 78238

Alan P. Morris Department of Geology, The University of Texas at San Antonio, San Antonio, Texas 78249

Sidney M. Jones
John A. Stamatakos Center for Nuclear Waste Regulatory Analyses, 6220 Culebra Road, San Antonio, Texas 78238

ABSTRACT

Results of new and previously published field and laboratory studies of the structural and geothermal evolution of Bare Mountain indicate a consistent structural plunge of 20-40° to the northeast that developed sometime between the Eocene and Middle Miocene. The plunge is pervasive at all scales throughout the central and northern parts of the mountain and is manifest by fault cutoff lines, fault branch lines, and fold and fault-block-tilt axes. Paleotemperature indicators confirm that tilting post-dates peak metamorphic conditions and most of the significant deformation within the mountain. Interpretations of pre-Miocene deformation and tectonism at Bare Mountain and adjacent Crater Flat, including Yucca Mountain, are considerably simplified by recognition of this plunge. The present orientation of faults and sense of apparent offset across faults within Bare Mountain suggest oblique, right-lateral strike-slip

displacement. Restoration of the plunge reveals that these faults are actually part of a system of formerly southeast-dipping listric normal faults with top-to-the-southeast displacement. These southeast-dipping normal faults were subsequently rotated to their present eastward dips by tilting (up to 40°) about a northwest-trending horizontal axis in the footwall breakaway of a regional detachment system that extends west and southwest of the southwest flank of Bare Mountain. The Eocene age of the faulting within Bare Mountain (prior to Miocene tuff deposition), and the location of Yucca Mountain within an area of regionally recognized pre-Middle Miocene extension, suggests that equivalent Paleozoic and Precambrian strata beneath the Miocene tuff section at Yucca Mountain may be cut by faults similar to those recognized in Bare Mountain. These faults are expected to dip steeply southeastward in their unrotated state (e.g., at depth beneath Yucca Mountain) and may provide blind seismic sources. The focus of the M5.6 1992 Little Skull Mountain earthquake was at a depth of about 10 km and occurred on a fault plane that strikes about 055 and dips 56° to the southeast. The Little Skull Mountain earthquake rupture plane is near the slip tendency maximum for faults in the contemporary stress field and is coincident with unrotated orientations of pre-Middle Miocene extensional faults at Bare Mountain. We conclude that the Little Skull Mountain earthquake occurred on a normal fault that formed during the Eocene and is probably part of a larger buried fault population within the pre-Tertiary strata of the region.

5/357
LH

INTRODUCTION

Bare Mountain is located in southwestern Nevada approximately 15 km west of Yucca Mountain, the proposed site for a permanent geological repository for high-level radioactive waste (Fig. 1). Bare Mountain is a block of Precambrian and Paleozoic metasedimentary rocks that provides a rare glimpse of the pre-Tertiary rocks existing beneath the Miocene tuffs of the Yucca Mountain area. Understanding the structural framework of Bare Mountain helps establish viable tectonic models for the region, and reveals the structural style in the pre-Tertiary strata beneath Yucca Mountain.

Bare Mountain forms the footwall of at least three post Eocene extensional fault systems: (1) a southwest-directed (top-to-the-southwest) extensional fault that exhumed the southwestern flank of Bare Mountain and unroofed Bare Mountain, (2) the Fluorspar Canyon Fault, and (3) the Bare Mountain Fault. The southwest-directed detachment system is most likely the principal structure responsible for exhumation of Bare Mountain and is probably related to the Bullfrog Hills/Boundary Canyon/Funeral Detachment system (Hamilton, 1988; Maldonado, 1990; Hoisch and Simpson 1993). The Fluorspar Canyon Fault is also part of the Bullfrog Hills Detachment system, a west-directed (top-to-the-west), extensional detachment system (Figs. 1 and 2) which was active during the Miocene (13-7.5 Ma) but after initial west- or southwest-directed detachment faulting. It may have accommodated as much as 275% extension of the Tertiary volcanic sequence within the Bullfrog Hills northwest of Bare Mountain (Hamilton, 1988; Carr and Monsen, 1988; Scott, 1990; Maldonado, 1990). The Bare Mountain Fault is an east-directed (top-to-the-east) normal fault, active from the Miocene into the Holocene (Snyder and Carr, 1984; Swadley et al., 1984; Carr and Parrish, 1985; Reheis, 1986; Ferrill et al., 1996b). It has previously been interpreted to cut a low angle west-directed extensional detachment at the base of the Tertiary sequence (Hamilton, 1988; Scott, 1990). However, considerable evidence now indicates that Bare Mountain has been exposed at least since the Middle Miocene (Carr and Parrish, 1985; Simonds et al., 1995; Spivey et al., 1995). We interpret

the Bare Mountain Fault as a listric normal fault which soles at depth into a low angle fault or ductile shear zone to the east (Ferrill et al., 1995; Ferrill et al. 1996a) and as such may directly control activity of Yucca Mountain faults. In this interpretation, faults mapped in the Miocene tuffs at Yucca Mountain accommodate hangingwall deformation related to motion along the Bare Mountain Fault.

Interpretations of Bare Mountain deformation history are complicated by the structural complexity involving contractional faulting and folding, several generations of extensional faulting, the possibility of significant vertical axis rotations, and ambiguities surrounding both timing of deformation and sense of fault slip. The general northward dip of strata, eastward dip of faults, and apparent strike slip and oblique slip on faults in Bare Mountain have been the source of much uncertainty with respect to the structural evolution of the range (Monsen, 1983; Monsen et al., 1992; Carr and Monsen, 1988).

In the present study we investigate structural style, timing constraints, and deformation history of faulting in order to evaluate the pre-Miocene tectonic history of Bare Mountain and implications of the resulting detailed deformation history for the neotectonic setting of Yucca Mountain. New structural and geothermal data coupled with previously published metamorphic data demonstrate that much of the apparent complexity of faulting within Bare Mountain is due to a previously unrecognized northeast plunge of the mountain. We invoke footwall deformation during early phases of top-southwest displacement along a southwest-dipping extensional fault in order to explain initial exhumation of the southwest flank of Bare Mountain and the resulting ~40° northeastward structural plunge. Viewed in this context, the western side of Bare Mountain exposes an oblique cross section through a northeast-plunging normal fault system. New timing constraints on early Tertiary extensional deformation within Bare Mountain provide insights into a previously unrecognized subregional fabric of southeast-dipping faults in the Paleozoic section which provides an analog for potential buried (blind) seismic sources in

the Yucca Mountain region. The 1992 Little Skull Mountain earthquake is considered as a possible example of slip on one such fault.

GEOLOGIC FRAMEWORK

Bare Mountain exposes a 7.4 km thick section of Late Proterozoic through Mississippian marine sedimentary rocks (Monsen et al., 1992) (Fig. 2). The pre-Tertiary sequence is part of the continental shelf miogeocline on the western margin of the North American craton in Late Proterozoic to Mississippian time (e.g., Poole et al., 1992; Burchfiel et al., 1992) (Fig. 2). The youngest Paleozoic strata exposed at Bare Mountain are Mississippian and Late Devonian (?) rocks exposed in northeast Bare Mountain. Older strata are exposed to the south and west. The Precambrian and Paleozoic strata have been intruded by minor Cretaceous, Oligocene, and Miocene intrusives (Monsen et al., 1992). Eruption of a variety of pyroclastic rocks, with minor rhyolitic flows and basalts, occurred during the Early and Middle Miocene (15–12.8 Ma; e.g., Sawyer et al., 1994), roughly coeval with the onset of extreme regional extension in the Basin and Range (Wernicke 1992).

Using metamorphic mineral assemblage, Monsen (1983) revealed highest metamorphic grades in the northwestern corner of Bare Mountain where the hangingwall of the subhorizontal Conejo Canyon Fault contains staurolite-bearing upper amphibolite facies Cambrian strata (peak temperature >520 °C) and is juxtaposed with biotite-zone greenschist facies Cambrian and late Proterozoic strata (peak temperature 350-400 °C) in the footwall. Another major fault that juxtaposes discordant metamorphic grades is the steep east-dipping Gold Ace Mine Fault (Fig. 2). Pelitic beds west of the Gold Ace Mine Fault tend to have strong slaty cleavage, whereas shale layers (in the Nopah Formation) east of the Gold Ace Mine Fault typically exhibit a non-penetrative planar cleavage that is clearly of lower grade. The non-metamorphosed appearance of shaly units east of the Gold Ace Mine Fault suggests sub-greenschist facies peak metamorphic conditions (<300 °C) for Cambrian and

Ordovician strata exposed immediately east of the Gold Ace Mine Fault. The juxtaposition of biotite-zone greenschist facies and sub-greenschist facies across the Gold Ace Mine fault represents ~100 °C difference in metamorphic temperature which equates to 3.3 km of vertical displacement, assuming an average Basin and Range geothermal gradient of 30°C/km (Sass et al., 1994). For comparison, the geologic cross section drawn across Bare Mountain indicates about 3.0 km of vertical displacement along the Gold Ace Mine Fault based on stratigraphic offset (Fig. 2).

Paleotemperature estimates from conodont color alteration index (CAI) data for Bare Mountain (Grow et al., 1994) show trends similar to those from metamorphic data. Lowest CAI values (4-4.5) found in northeastern Bare Mountain (at Meiklejohn Peak) correlate to maximum temperatures of 190-250 °C (Harris et al., 1978; Grow et al., 1994). Conodont CAI values from south and west of Meiklejohn Peak generally range between 5 and 7 which indicate peak temperatures >300 °C (Grow et al., 1994; Rehebian et al., 1987). In comparison, conodonts from samples of Paleozoic carbonates from borehole UE25 #P1 at Yucca Mountain yielded CAI value of 3 (Grow et al. 1994), indicating peak temperature of 110-200 °C (after Harris et al. 1978), considerably lower than any peak temperature estimate from Bare Mountain. This contrast shows considerably shallower maximum burial for Paleozoic rocks at Yucca Mountain.

Lower-temperature constraints on faulting and exhumation are provided by apatite fission track results from samples in similar lithologies to those used in the higher temperature analyses (Ferrill et al., 1995a; Spivey et al., 1995). Apatite fission tracks anneal at temperatures above 110 °C, and therefore constrain the age of cooling (exhumation) of Bare Mountain through the 110 °C geotherm. Fission track ages from Bare Mountain average 15 Ma and indicate exhumation in the Middle Miocene (Ferrill et al. 1996a; Spivey et al., 1995). There are no significant offsets of apatite ages across either the Gold Ace Mine or Conejo Canyon faults. Thus, significant fault displacements recorded by

9/3 $7
LH

the metamorphic and conodont temperature data must have occurred prior to the Middle Miocene.

FAULTS WITHIN BARE MOUNTAIN

Pre-Tertiary deformation within Bare Mountain is represented by contractional structures that include the Meiklejohn Peak Thrust, the Panama Thrust, and perhaps the Conejo Canyon Detachment system (Snow, 1992; Caskey and Schweickert, 1992). Displacement histories of the Meiklejohn Peak and Conejo Canyon faults are complicated by reactivation as extensional faults during the Tertiary (Monsen et al., 1992). The dominant internal structure of present day Bare Mountain is characterized by bedding that dips to the north and extensional faults that dip to the east and have *apparent* offsets that suggest right-lateral strike-slip or oblique-slip (Monsen, 1983; Carr and Monsen, 1988; Monsen et al., 1992). The largest displacement fault of the east-dipping set is the Gold Ace Mine Fault (Fig. 2). K-Ar dating of muscovite and biotite from schists of the Wood Canyon Formation in northwest Bare Mountain and southeast Bullfrog Hills (Monsen et al., 1992; Axen et al., 1993) indicates cooling during the Eocene (44-52 Ma). This cooling is attributed to tectonic exhumation by displacement along the Gold Ace Mine Fault and other east-dipping faults.

The subhorizontal Conejo Canyon Detachment contains a dismembered sequence of uppermost Late Proterozoic to lowermost Paleozoic rocks in its hangingwall and apparently cuts faults of the predominant east-dipping (Eocene) fault set (Monsen et al., 1992). Structural and metamorphic relationships described and mapped by Monsen (1983), Carr and Monsen (1988), and Monsen et al. (1992) illustrate the complex geologic relationships of the Conejo Canyon Detachment system. Juxtaposition of staurolite-bearing strata over garnet-bearing strata suggests contractional displacement, whereas removal of stratigraphic section suggests extensional displacement. Regardless of actual displacement path(s) of the Conejo Canyon Detachment system, consistency of timing of exhumation in the Middle

Miocene as constrained by apatite fission track thermochronometry indicates that major displacement on the Conejo Canyon Detachment system was prior to apatite closure (110 °C) at 15 Ma.

STRUCTURAL ANALYSIS

Several types of structural data constrain horizontal-axis tilting of Bare Mountain, including outcrop and large scale fold axes, fault-bedding intersections, cleavage-bedding intersections, and synthetic and antithetic fault intersections. Bedding orientations from Bare Mountain (from Monsen et al., 1992), contoured and fitted by best-fit great circles (Fig. 3), define a northeastward plunge to the axis of bedding tilt in northern and central Bare Mountain, and an eastward plunge in southern Bare Mountain. The overall bedding tilting is the composite result of both folding and fault block tilting. Bedding orientations around the large late Paleozoic contractional fold at Meiklejohn Peak (Fig. 4) define a 33° plunge toward 039 (Fig. 4).

Bedding cutoff lines on early Tertiary faults at virtually all scales within Bare Mountain have similar plunges. The intersection between the dominant north dip of bedding in central and northern Bare Mountain (Fig. 3) and east dip of extensional faults, such as the Gold Ace Mine Fault, plunges northeastward. At well-exposed outcrops, fault and bedding intersections clearly demonstrate the northeastward plunge. For example, fault and bedding orientations from an extensional fault system exposed in the hangingwall of the Gold Ace Mine Fault define a plunge of 37° toward 042 (Fig. 5). This plunge of fault and bedding intersections in the hangingwall of the Gold Ace Mine Fault persists down to the mesoscopic scale where small faults intersect bedding to define a northeastward plunge of 36° toward 041 (Fig. 6). The fact that this plunge is so consistently developed, defined by structures from cm to km scale, and defined by structures spanning late Paleozoic through Tertiary ages suggests that the structural plunge was developed after significant compressional and extensional deformation.

CALCITE DEFORMATION GEOTHERMOMETRY

Calcite deformation geothermometry shows a pattern of increasing deformation temperature from northeast to southwest that also indicates a northeast plunge of Bare Mountain. Calcite deformation geothermometry utilizes the temperature dependence of calcite twinning and recrystallization to estimate temperatures during deformation. During deformation, twin nucleation and twin growth (widening) occur simultaneously, but at different rates (Ferrill, 1991; Burkhard, 1993). As temperatures increase (>150-200 °C), growth by twin widening is favored over twin nucleation. Dynamic recrystallization becomes the favored mechanism of calcite deformation at even higher temperatures (>250 °C). Several distinct temperature regimes for twinning and recrystallization have been identified empirically (Ferrill, 1991; Burkhard, 1993).

Samples for this study were collected from Cambrian through Devonian carbonates from sites distributed throughout Bare Mountain (Fig. 7). Oriented thin sections were then prepared and examined optically using a standard petrographic microscope to characterize the dominant twin types. Deformation temperatures were inferred using the approach of Burkhard (1993) in which the first appearance of microstructures is used as the basis for estimating peak deformation temperature.

The distribution of calcite microstructures provides evidence for several distinct deformation temperature domains within Bare Mountain (Fig. 7). Complete recrystallization and type IV twins (e.g., thick, patchy, and recrystallized twins), indicating deformation temperatures >250 °C, are found near the Gold Ace Mine Fault (location A in Fig. 7) along the southwestern flank of Bare Mountain, and in the northwest corner of Bare Mountain (consistent with high temperatures recorded by metamorphic mineral assemblages and conodont CAI data). Twin types II (thick tabular twins) and III thick, curved and tapered twins), indicating deformation temperatures of 150 to 250 °C, are common in the central portions of Bare Mountain (location B in Fig. 7) and south of the

Panama Thrust. Type I twins (straight thin twins), which indicate deformation temperatures < 200 °C, predominate only in the northeast corner of Bare Mountain (locations C and D in Fig. 7), within and near Meiklejohn Peak. These calcite microstructural data indicate lowest deformation temperatures in the northeast corner of Bare Mountain, and progressively higher maximum deformation temperatures to the south and west.

DEVELOPMENT OF NORTHEAST PLUNGE

The northeastward plunge of Bare Mountain is best explained by northeastward tilting of the Bare Mountain block after formation of the structures and acquisition of metamorphic- and deformation-temperature gradients within Bare Mountain. The amount of tilting can be independently estimated from calcite deformation data projected along a southwest-northeast traverse from the Gold Ace Mine to Meiklejohn Peak Faults. These sites, except for one from the hangingwall of the Meiklejohn Thrust, are situated within an unbroken (by faulting) fault block and thus comprise a single stratigraphic section. The distribution shows a 100–150 °C difference in peak deformation temperature at sites that are currently at about the same elevation (Fig. 8). To obtain sub-horizontal geotherms, the profile can be restored by tilting Bare Mountain to the southwest about a northwest-southeast horizontal axis. A realistic range of geothermal gradients (24 to 50 °C/km; Sass et al., 1994) is obtained when Bare Mountain is back-tilted between 30° and 45° which also restores structural plunge to 0°. Such a restoration assumes that the temperature-dependent microstructures formed rapidly in a regime of horizontal geotherms. The inferred range of geothermal gradients indicates that the calcite twins formed at depths between 3 and 10 km below the surface. This deformation was followed by northeast tilting and uplift of Bare Mountain which exposed the calcite microstructures in their present outcrops.

The age of tilting of Bare Mountain is bracketed between the Eocene and Middle Miocene, based on apatite fission track ages (Spivey et al., 1995), K/Ar ages from schists

of the Wood Canyon Formation (Monsen et al., 1992), paleomagnetic data from the contractional fold at Meiklejohn Peak (Fig. 4) in northeastern Bare Mountain and paleomagnetic data from a dated mafic dike in northwestern Bare Mountain (Ferrill et al., 1995). Apatite fission track data constrain the timing of relatively uniform cooling of northern Bare Mountain through ~110 °C in the Middle Miocene. Calcite microstructures in the present study indicate deformation temperatures in western Bare Mountain in excess of 250 °C, which shows that this deformation occurred prior to the Middle Miocene uplift recorded in the apatite grains. In contrast, paleomagnetic results demonstrate that northeast tilting occurred after acquisition of a post-folding Permian-Triassic secondary magnetization of the Paleozoic carbonates in the Meiklejohn Peak fold (Ferrill et al., 1995).

Additional paleomagnetic data from an Oligocene mafic dike in northwestern Bare Mountain further refine the timing of tilting to the northeast. These results show a two polarity magnetization that coincides with the expected Tertiary direction for Nevada. However, the direction is obtained without correction for the 40° plunge suggesting that the plunge predates dike intrusion. Age of the mafic dike is problematic in that biotite yielded an age of 16.6 ± 1.2 Ma and hornblende yielded 26.1 ± 1.7 Ma (Monsen et al., 1992). Given the cooling history suggested by other geothermometric results discussed previously, these ages may also represent regional cooling of Bare Mountain and not original dike emplacement. Thus, regardless of the original age, we suggest that the dike, along with western Bare Mountain, cooled considerably in the Middle Miocene. In this scenario, the two-polarity magnetization probably reflects a partial thermal remanent magnetization acquired as the dike cooled. Thus, tilting of Bare Mountain occurred prior to the Middle Miocene.

Pre-Middle Miocene tilting of Bare Mountain preferentially exhumed progressively deeper, older, and hotter strata from northeast to southwest. Northeast tilting during or prior to the Middle Miocene is best explained as produced by footwall uplift beneath a top-to-the-southwest breakaway normal fault (e.g., Wernicke and Axen 1988; Wernicke, 1992;

Fig. 9). The southwest flank of Bare Mountain in this interpretation represents the breakaway for the Bullfrog Hills/Boundary Canyon/Funeral Detachment system. In Wernicke and Axen's (1988) model, footwall tilting of the breakaway occurs relatively early in response to isostatic footwall uplift associated with exhumation by the detachment. Footwall exhumation is progressively younger from the breakaway towards the hangingwall. Apatite fission track data from the lower plate of the Bullfrog Hills/Boundary Canyon/Funeral Detachment system (Fig. 9) indicate a general westward younging of cooling ages that indicate closure at 15 Ma from Bare Mountain (Ferrill et al., 1996a; Spivey et al., 1995), 10 Ma from the Bullfrog Hills (Hoisch et al., in review), and 6 Ma from the Funeral Mountains (Holm and Dokka, 1991; Hoisch et al., in review).

IMPLICATIONS FOR NEOTECTONICS OF THE YUCCA MOUNTAIN REGION

The role of listric faulting in the Bare Mountain and Yucca Mountain area has been the source of considerable debate (e.g., Simonds et al., 1996) because of its potential for shallow seismic sources represented by shallow fault systems and the possibility that shallow fault systems mask deeper, blind seismic sources. Cross sections by Young et al. (1993) and Ferrill et al. (1996a), based on geometric constraints, indicate the possibility of listric faults in the middle and lower parts of the brittle crust (within the pre-Tertiary section) beneath Yucca Mountain. Recent mechanical modeling indicated that such listric faults could be active in the present regional stress field. However, the potential for seismicity is considerably smaller on low angle fault segments than on steep segments, due to reduced rupture propagation rate on low angle fault segments (Ofoegbu and Ferrill, 1995). The present study documents that listric fault systems that flatten from steep to shallow depths within the Paleozoic and Precambrian stratigraphic section produce the dominant structural fabric within Bare Mountain. As discussed by Elliott (1983), balanced structural models must be both admissible (constructed using the structural style observable

earthquake magnitude and fault rupture area of Wells and Coppersmith (1994), a magnitude 5.6 earthquake represents a rupture area of approximately 36 km^2. A 36 km^2 circular rupture of this area would have a diameter of 6.8 km. The cross section in Figure 2 illustrates that several of the faults within Bare Mountain extend in the dip direction for more than 7 km and suggests that faults of this and larger dimensions are probably prevalent beneath the Miocene tuff cover between Bare Mountain and Little Skull Mountain beneath Crater Flat, Yucca Mountain, and Jackass Flat (Fig. 1).

CONCLUSIONS

Structures within Bare Mountain were tilted approximately 30-40° toward the northeast, after southeast directed Eocene extension. This tilting rotated southeast-dipping normal faults to their present eastward dips. Recognition of this tilting explains the structural plunge and lateral metamorphic- and deformation-temperature variations within the mountain. Tilting represents deformation in the footwall of a southwest-directed extensional breakaway that exhumed the southwestern flank of Bare Mountain and produced the northeast tilt by footwall uplift. Bare Mountain provides the best exposed examples of deformation within the pre-Tertiary sequence in the immediate vicinity of Yucca Mountain. The southwestern flank of Bare Mountain exposes a cross section approximately normal to structural plunge within the mountain and illustrates that the normal faults within the mountain merge and flatten with depth to form a listric fan. The apparent right-lateral strike-slip and oblique-slip displacements on east-dipping faults in Bare Mountain actually developed as normal dip-slip displacements on southeast-dipping normal faults accommodating northwest-southeast extension. The structural history of Bare Mountain likely represents a common structural style for the pre-Tertiary section and should be considered in development and assessment of admissibility of structural models for the region. Southeastward-dipping normal faults are expected to be prevalent within the pre-Tertiary section beneath the volcanic cover in the Yucca Mountain area. The 1992

in the region) and viable (restorable to an unstrained state). Inasmuch as Bare Mountain represents the most complete exposure of the pre-Tertiary section in close proximity to Yucca Mountain, the structural style observed in Bare Mountain must be considered as a primary constraint for developing and assessing admissibility of structural models for the pre-Tertiary rocks in the surrounding area.

Timing constraints on the formation of early extensional faults in Bare Mountain indicate that faulting occurred considerably earlier than Miocene tuff deposition, formation of the Bare Mountain Fault, and faulting at Yucca Mountain and Crater Flat. Bare Mountain is within a pre-Middle Miocene extensional province defined by Axen et al. (1993) which extends from the Grapevine Mountains (25 km west of Bare Mountain) to 100 km east of Bare Mountain. The implication of the relatively early normal faulting is that similar faults probably exist east of Bare Mountain, for example beneath Crater Flat, Yucca Mountain, and Jackass Flat. We interpret the northeast tilting of the faults at Bare Mountain as a local product of footwall tilting due to regional detachment faulting that has not extended eastward as far as Yucca Mountain. Therefore, in order to understand the sub-Tertiary structural fabric at Yucca Mountain, the fault orientations at Bare Mountain must restored to their pre-tilt orientation. For example, restoring faults exposed near Gold Ace Mine Fault (shown in Fig. 5) to their pre-tilt orientation indicates that the faults originally dipped to the southeast. These tilt-corrected orientations cluster near the maximum slip tendency in the contemporary stress field (Fig. 10; Morris et al., 1996). A possible example of slip on one such fault is the 1992 Little Skull Mountain earthquake.

The focus of the M5.6 1992 Little Skull Mountain earthquake was at a depth of about 10 km (Fig. 10; Harmsen, 1994). Nodal planes from the Little Skull Mountain earthquake and aftershocks indicate that the slip occurred on faults clustered around the slip tendency maximum in the contemporary stress field (Fig. 10). The Little Skull Mountain mainshock occurred on a southeast-dipping fault (Harmsen 1994) analogous to the faults of the east-dipping set seen in Bare Mountain. Based on scaling relationships between

M5.6 Little Skull Mountain earthquake and associated aftershocks represent seismic slip on faults in the pre-Tertiary sequence in orientations independently indicated based on structural data from Bare Mountain. Although these faults may largely be blind and therefore difficult to detect, they may be contributors to background seismicity in the Yucca Mountain region.

ACKNOWLEDGMENTS

This paper was prepared as a result of work performed at the Center for Nuclear Waste Regulatory Analyses (CNWRA) for the U.S. Nuclear Regulatory Commission (NRC) under contract number NRC-02-93-005. The activities reported here were initiated on behalf of the NRC Office of Nuclear Regulatory Research, as part of the Tectonic Processes of the Central Basin and Range research project, and continued on behalf of the Office of Nuclear Material Safety and Safeguards. This paper is an independent product of the CNWRA and does not necessarily reflect the views or regulatory position of the NRC. We wish to thank Brent Henderson, Kathy Spivey, Ron Martin, Steve Young, Larry McKague, Aaron Kullman, Barbara Long, and Esther Cantu for their critical comments and assistance in manuscript preparation. Technical reviews by Gerry Stirewalt and Wes Patrick considerably improved the manuscript. We thank Anita Harris (U.S. Geological Survey) for supplying conodont data from Bare Mountain.

REFERENCES CITED

Axen, G.J., Taylor, W.J., and Bartley, J.M. 1993, Space-time patterns and tectonic controls of Tertiary extension and magmatism in the Great Basin of the western United States: Geological Society of America Bulletin, v. 105, p. 56–76.

Burchfiel, B.C., Cowan, D.S., and Davis, G.A., 1992, Tectonic overview of the Cordilleran orogen in the western United States, *in* Burchfiel, B.C., Lipman, P.W., and Zoback, M.L., eds., The Cordilleran orogen: Conterminous U.S.:

Boulder, Colorado, Geological Society of America, Geology of North America, v. G-3, p. 407–479.

Burkhard, M., 1993, Calcite twins, their geometry, appearance and significance as stress-strain markers and indicators of tectonic regime: A review: Journal of Structural Geology, v. 15, p. 351–368.

Carr, M.D., and Monsen, S.A., 1988, A field trip guide to the geology of Bare Mountain, *in* Weide, D.L., and Faber, M.L., eds., This extended land: Geological Society of America Cordilleran Section Meeting, Field Trip Guidebook: University of Nevada at Las Vegas Geoscience Department Special Publication 2, p. 50–57.

Carr, W.J., and Parrish, L.D., 1985, Geology of Drill Hole USW-VH-2, and Structure of Crater Flat, Southwestern, Nevada: U.S. Geological Survey Open-File Report 85-475.

Caskey, S.J., and Schweickert, R.A., 1992, Mesozoic deformation in the Nevada Test Site and vicinity: Implications for the structural framework of the Cordilleran fold and thrust belt and Tertiary extension north of Las Vegas Valley: Tectonics, v. 11, p. 1314–1331.

Elliott, D., 1983, The construction of balanced cross sections: Journal of Structural Geology, v. 5, p. 101.

Ferrill, D.A., 1991, Calcite twin widths and intensities as metamorphic indicators in natural low temperature deformation of limestone: Journal of Structural Geology, v. 13, p. 667–675.

Ferrill, D.A., Morris, A.P., Stamatakos, J.A., and Spivey, K.H., 1995, Tectonic processes in the central Basin and Range region, *in* Sagar, B., ed., NRC High-Level Radioactive Waste Research at CNWRA, July-December 1994. Center for Nuclear Waste Regulatory Analyses, San Antonio, Texas, p. 6-1–6-27.

Ferrill, D.A., Stirewalt, G.L., Henderson, D.B., Stamatakos, J.A., Morris, A.P. Wernicke, B.P., and Spivey, K.H., 1996a, Faulting in the Yucca Mountain Region:

17/9/35

Critical Review and Analyses of Tectonic Data from the Central Basin and Range, CNWRA 95-017, NUREG/CR-6401: U.S. Nuclear Regulatory Commission, Washington, D.C.

Ferrill, D.A., Stamatakos, J.A., Jones, S.M., Rahe, B., McKague, H.L., Martin, R.H., and Morris, A.P., 1996b, Quaternary slip history of the Bare Mountain Fault (Nevada) from the morphology and distribution of alluvial fan deposits: Geology, v. 24, p. 559-562.

Fisher, R.A., 1953, Dispersion on a sphere. Proceedings of the Royal Astronomical Society of London A217, p. 295–305.

Grow, J.A., Barker, C.E., and Harris, A.G., 1994, Oil and gas exploration near Yucca Mountain, southern Nevada, in International High-Level Radioactive Waste Management Conference Proceedings, American Nuclear Society, La Grange Park, Illinois, p. 1298–1315.

Hamilton, W.B., 1988, Detachment faulting in the Death Valley region, California and Nevada, *in* Carr, M.D., and Yount, J.C. eds., Geologic and Hydrologic Investigations of a Potential Nuclear Waste Disposal Site at Yucca Mountain, Southern Nevada: U.S. Geological Survey Bulletin 1790, p. 51–85.

Harmsen, S.C., 1994, The Little Skull Mountain, Nevada, earthquake of 29 June 1992: Aftershock focal mechanisms and tectonic stress field implications: Bulletin of the Seismological Society of America, v. 84, p. 1484–1505.

Harris, A.G., Harris, L.D., and Epstein, J.B., 1978, Oil and gas data from Paleozoic rocks in the Appalachian Basin: Maps for assessing hydrocarbon potential and thermal maturity (conodont color alteration isograds and overburden isopachs): U.S. Geological Survey Miscellaneous Investigations Series Map I-917E, scale 1:2,500,000.

Hoisch, T.D., Heizler, M.T., and Zartman, R.E. (in review). Timing of detachment faulting west of Yucca Mountain, Nevada: Inferences from $^{40}Ar/^{39}Ar$, K-Ar, U-Pb and fission-track thermochronology. Journal of Geophysical Research.

Hoisch, T.D., and Simpson, C., 1993. Rise and tilt of metamorphic rocks in the lower plate of a detachment in the Funeral Mountains, Death Valley, California. Journal of Geophysical Research, v. 98, p. 6805-6827.

Holm, D.K., and Dokka, R.K. 1991. Major late Miocene cooling of the middle crust associated with extensional orogenesis in the Funeral Mountains, California. Geophysical Research Letters, v. 18, p. 1775-1778.

Maldonado, F., 1990, Structural geology of the upper plate of the Bullfrog Hills detachment fault system, southern Nevada: Geological Society of America Bulletin, v. 102, p. 992–1006.

Monsen, S.A., 1983, Structural evolution and metamorphic petrology of the Precambrian-Cambrian strata, northwest Bare Mountain, Nevada: Davis, California, University of California at Davis, Masters Thesis, 66 p.

Monsen, S.A., Carr, M.D., Reheis, M.C., Orkild, P.A., 1992, Geologic Map of Bare Mountain, Nye County, Nevada: U.S. Geological Survey Miscellaneous Investigations Series, Map I-2201, scale 1:24 000.

Morris, A.P., Ferrill, D.A., and Henderson, D.B., 1996, Slip tendency analysis and fault reactivation. Geology, v. 24, 275–278.

Ofoegbu, G.I., and Ferrill, D.A., 1995, Mechanical analyses of a Yucca Mountain fault model, in Proceedings, Topical Meeting on Methods of Seismic Hazards Evaluation, Focus '95, Las Vegas, Nevada, American Nuclear Society, p. 115–124.

Poole, F.G., Stewart, J.H., Palmer, A.R., Sandberg, C.A., Madrid, R.J., Ross, R.J., Jr., Hintze, L.F., Miller, M.M., and Wrucke, C.T., 1992, Latest Precambrian to latest Devonian time; Development of a continental margin, *in* Burchfiel, B.C.,

Lipman, P.W., and Zoback, M.L., eds., The Cordilleran orogen: Conterminous United States: Boulder, Colorado, Geological Society of America, Geology of North America, v. G-3, p. 407–479.

Ramsay, J.G., 1967, Folding and fracturing of rocks: London, McGraw-Hill.

Rehebian, V.A., Harris, A.G., and Huebner, J.S., 1987, Conodont color and textural alteration: An index to regional metamorphism, contact metamorphism, and hydrothermal alteration: Geological Society of America Bulletin, v. 99, p. 471–479.

Reheis, M.C., 1986, Preliminary study of Quaternary faulting on the east side of Bare Mountain, Nye County, Nevada, *in* Geologic and Hydrologic Investigations of Yucca Mountain, Nevada.: U.S. Geological Survey Open-File Report 86-576, p. 103–111.

Sass, J.H., Lachenbruch, A.H., Galanis, S.P., Jr., Morgan, P., Priest, S.S., Moses, T.H., Jr., and Munroe, R.J., 1994, Thermal regime of the southern Basin and Range Province: Heat flow data from Arizona and the Mojave Desert of California and Nevada: Journal of Geophysical Research, v. 99 (B11), p. 22093–22229.

Sawyer, D., Fleck, R.J., Lanphere, M.A., Warren, R.G., Broxton, D.E., and Hudson, M., 1994, Episodic caldera volcanism in the Miocene southwestern Nevada volcanic field: Revised stratigraphic framework, $^{40}Ar/^{39}Ar$ geochronology and implications for magmatism and extension: Geological Society of America Bulletin, v. 106, 1304–1318.

Scott, R.B., 1990, Tectonic setting of Yucca Mountain, southwest Nevada, *in* Wernicke, B.P., ed., Basin and Range extensional tectonics near the latitude of Las Vegas, Nevada: Boulder, Colorado, Geological Society of America Memoir 176, p. 251–282.

Simonds, F.W., Fridrich, C.J., Hoisch, T.D., and Hamilton, W.B., 1995, A synthesis of detachment fault studies in the Yucca Mountain Region, in Proceedings, Topical

Meeting on Methods of Seismic Hazards Evaluation, Focus '95, Las Vegas, Nevada, American Nuclear Society, p. 107–114.

Snow, J.K., 1992, Large-magnitude Permian shortening and continental-margin tectonics in the southern Cordillera: Geological Society of America Bulletin, v. 104, p. 80–105.

Snyder, D.B. and Carr, W.J., 1984, Interpretation of gravity data in a complex volcano-tectonic setting, south-western Nevada: Journal of Geophysical Research, v. 89, p. 10,193–10,206.

Spivey, K.H., Ferrill, D.A., Stamatakos, J., Morris, A.P., Donelick, R.A., and Young, S.R., 1995. Uplift and cooling history of Bare Mountain, Nevada, from apatite fission track thermochronology. Geological Society of America Abstracts with Programs, v. 27, no. 6, p. A-389.

Swadley, W.C., Hoover, D.L., Rosholt, J.N., 1984, Preliminary report on late Cenozoic faulting and stratigraphy in the vicinity of Yucca Mountain, Nye County, Nevada: U.S. Geological Survey Open-file Report 84-788, 42 p.

Wells, D.L., and Coppersmith, K.J., 1994, New empirical relationships among magnitude, rupture length, rupture width, rupture area, and surface displacement: Seismological Society of America Bulletin, v. 84, p. 974–1002.

Wernicke, B., and Axen, G.J. 1988. On the role of isostasy in the evolution of normal fault systems. Geology, v. 16, p. 848-851.

Wernicke, B., 1992, Cenozoic extensional tectonics of the U.S. Cordillera, *in* Burchfiel, B.C., Lipman, P.W., and Zoback, M.L., eds., The geology of North America, Volume G3: The Cordilleran orogen; Conterminous United States: Boulder, Colorado, Geological Society of America, p. 553–581.

Woodcock, N.H., 1977, Specification of fabric shape using an eigenvalue method: Geological Society of America Bulletin, v. 88, 1231–1236.

23/357

Young, S.R., Morris, A.P., Stirewalt, G., 1993, Geometric analysis of alternative models of faulting at Yucca Mountain, Nevada: in International High-Level Radioactive Waste Management Conference Proceedings, American Nuclear Society, La Grange Park, Illinois, p. 1818–1825.

24/357

FIGURE CAPTIONS

Figure 1. Simplified geologic map showing relationship of Bare Mountain with respect to Crater Flat, Yucca Mountain, and Little Skull Mountain. Dashed line labeled LSM indicates surface projection of blind rupture plane of the 1992 M5.6 Little Skull Mountain earthquake. Star shows epicenter of Little Skull Mountain earthquake (after Harmsen 1994).

Figure 2. (A) Geological map of Bare Mountain (after Monsen et al., 1992) showing the line of section A-A'. (B) Plunge-perpendicular cross section of Bare Mountain along section line A-A' (after Ferrill et al., 1995).

Figure 3. Structural domain map of Bare Mountain based on data in Monsen et al., (1992). Domain boundaries are drawn primarily on the basis of major faults. Lower hemisphere, equal-area stereographic projections are plotted for poles to bedding for each domain. Stars represent the poles to the best-fit great-circles (minimum eigenvector of the distribution) and represent the averaged fold axis for each domain (Fisher, 1953; Ramsay, 1967; Woodcock, 1977).

Figure 4. (A) Photograph of Meiklejohn Peak fold, northeastern Bare Mountain. (B) Interpreted photograph of the Meiklejohn Peak fold. Inset lower hemisphere, equal-area stereographic projection illustrates poles to bedding (squares). The northeastward plunge of Meiklejohn Peak fold axis (dot) is defined by pole to best-fit great circle for poles to bedding.

25/357
24

Figure 5. (A) Oblique areal photograph of western Bare Mountain northwest of Carrara Canyon. (B) Interpreted photograph. Inset lower hemisphere equal area stereographic projection illustrates poles to normal faults (triangles) and poles to antithetically dipping bedding (squares) on an equal area, lower hemisphere stereographic projection. The best-fit great circle fits poles to faults and bedding and defines the northeastward plunge of the intersection of faults and bedding (dot) at this exposure.

Figure 6. Field sketch and lower hemisphere equal area stereographic projection of bedding and mesoscopic extensional faults in Bare Mountain. Inset stereonet illustrates poles to normal faults (triangles) and poles to antithetically dipping bedding (squares) on an equal area, lower hemisphere projection. The best-fit great circle fits poles to faults and bedding and defines the northeastward plunge of the intersection of faults and bedding (dot) at this exposure.

Figure 7. Map of calcite-twin geothermometry sample sites with photomicrographs illustrating representative microstructures. (A) Complete recrystallization of calcite indicates deformation temperature >>250 °C. (B) Thick twins and the presence of dynamically recrystallized calcite indicate deformation temperature >250 °C. Dominance of crystal-plastic deformation by thin twins illustrated in (C) and (D) indicates low temperature deformation at temperatures <200 °C. Calcite microstructures indicate lowest deformation temperature in the northeast corner of Bare Mountain and laterally increasing deformation temperatures toward the south and west across the mountain.

Figure 8. Calcite-deformation geothermometry results across Bare Mountain: (A) Southwest-northeast topographic profile from the Gold Ace Mine to Meiklejohn Peak (inclined lines indicate inclined isotherms for a 30°, 45°, or 60° plunge of Bare Mountain to the northeast). (B) Topographic profile in A restored for a 30°, 45°, and 60° plunge showing predicted distribution of horizontal geotherms.

Fig. 9. Conceptual model of the development and evolution of extensional detachment breakaway zone along the southwest flank of Bare Mountain (modified after Wernicke and Axen, 1988). Details of faulting and deformation in the Neogene volcanic and sedimentary cover are not illustrated in order to emphasize larger-scale deformational features of the pre-Tertiary sequence. BMF = Bare Mountain Fault, BH = Bullfrog Hills, FM = Funeral Mountains, BM = Bare Mountain, and YM = Yucca Mountain.

Fig. 10. (A) Slip tendency plot for Yucca Mountain area (after Morris et al. 1996) with poles to faults from Gold Ace Mine exposure in southwestern Bare Mountain (Fig. 5B; after removal of northeastward plunge) and pole to M5.6 1992 Little Skull Mountain rupture plane overlain. (B) Slip tendency plot for Yucca Mountain overlaid with poles to nodal planes for the Little Skull Mountain earthquake and aftershocks illustrates close agreement between actual slipped planes and orientations of predicted high slip tendency (yellow to red colors). White triangles are poles to selected nodal planes and black triangles are poles to alternate planes as chosen by Harmsen (1994).

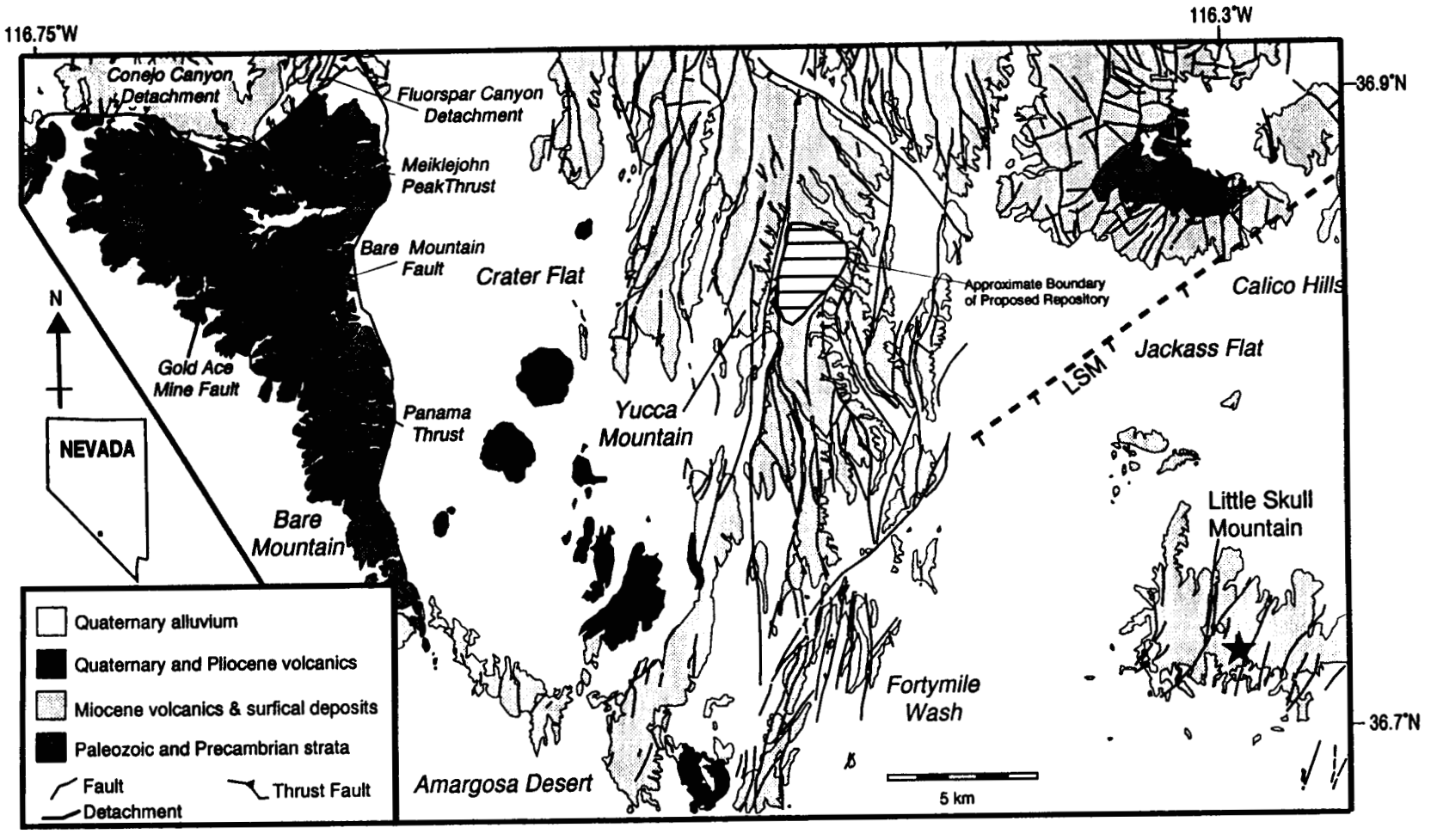

Ferrill et al.
Fig 1

23/35

28/387
JH

A

KEY:

- Faults
- Late Miocene alluvium and colluvium
- Miocene volcanics and intercalated gravel
- Miocene quartz latite dike
- Oligocene diorite dike
- Cretaceous granite
- Mississippian-Devonian Eleana Formation
- Devonian Fluorspar Canyon Formation
- Devonian Tarantula Canyon Formation
- Silurian Lone Mountain Dolomite
- Silurian Roberts Mountain Formation
- Ordovician Ely Springs Dolomite
- Ordovician Eureka Quartzite
- Ordovician Antelope Valley Formation
- Ordovician Ninemile Formation
- Ordovician Goodwin Limestone
- Cambrian Nopah Formation
- Cambrian Bonanza King Formation
- Cambrian Carrara Formation
- Cambrian Zabriskie Quartzite
- Cambrian-Precambrian Wood Canyon Formation
- Late Proterozoic Stirling Quartzite

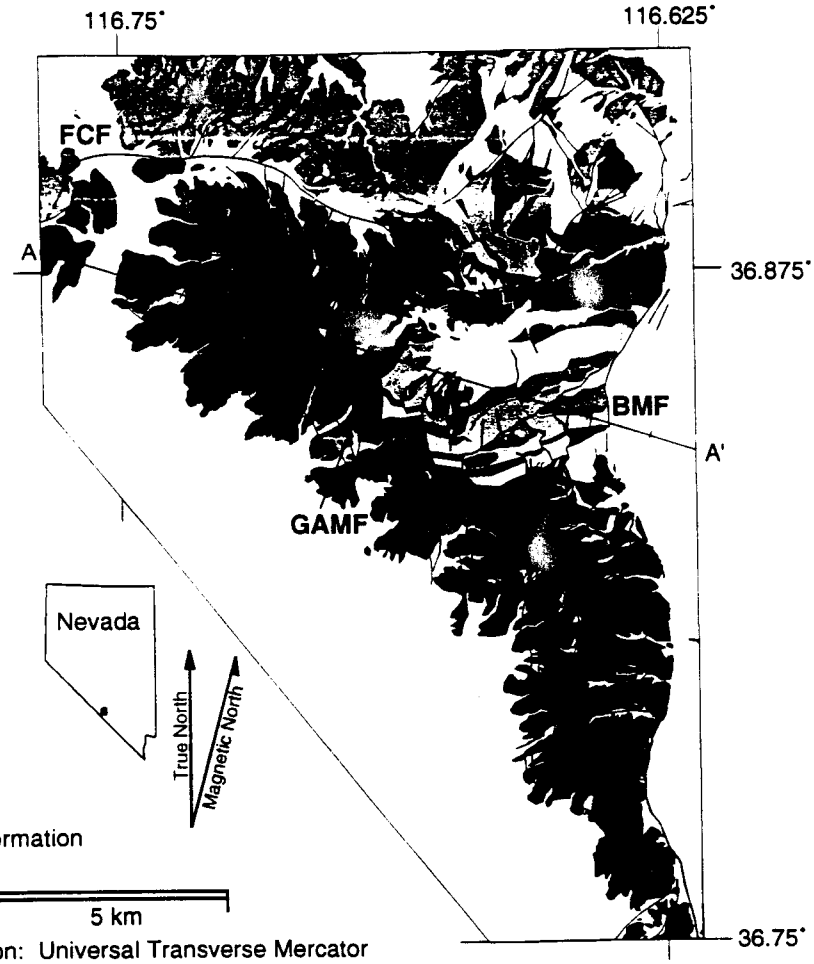

Projection: Universal Transverse Mercator

Ferrill et al.
Fig. 2

29/357
KH

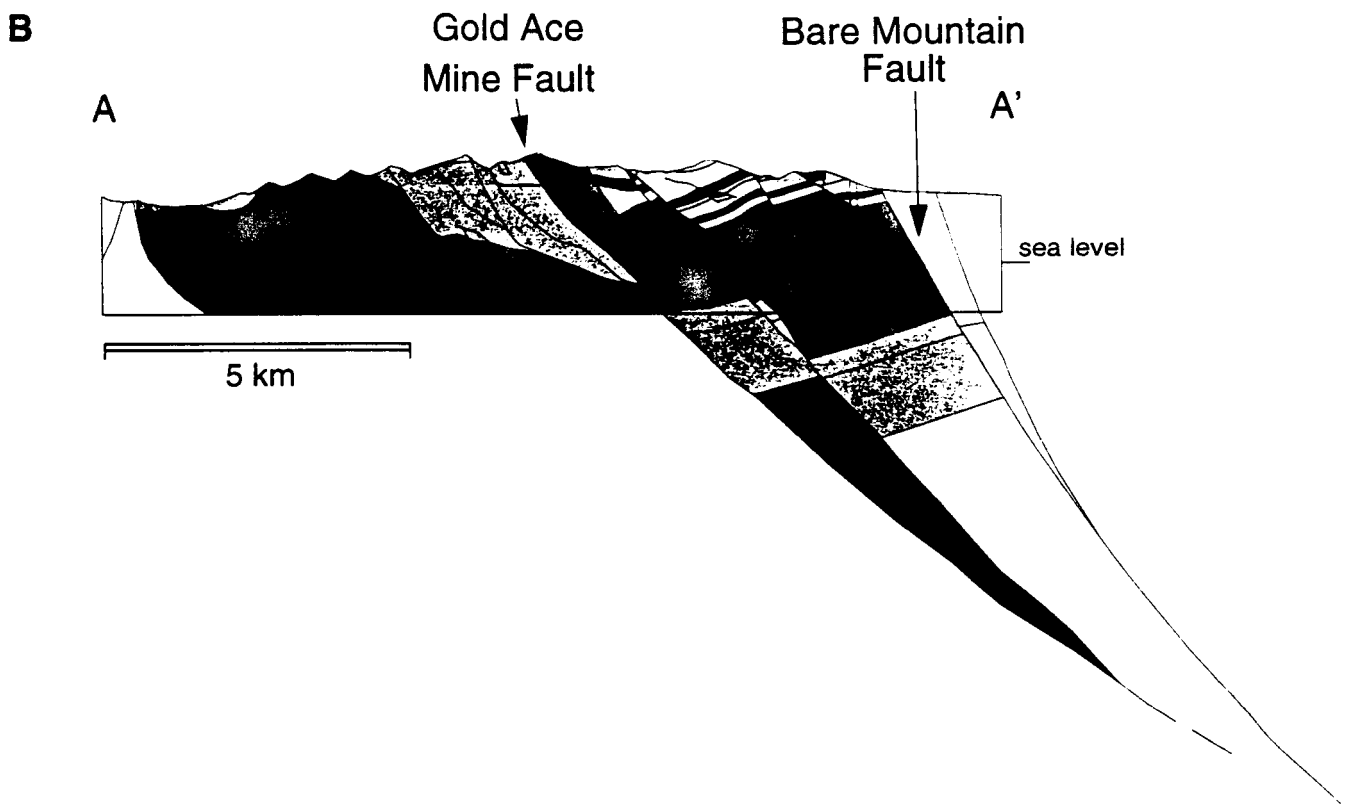

Ferrill et al.
Fig. 2

30/387
JH

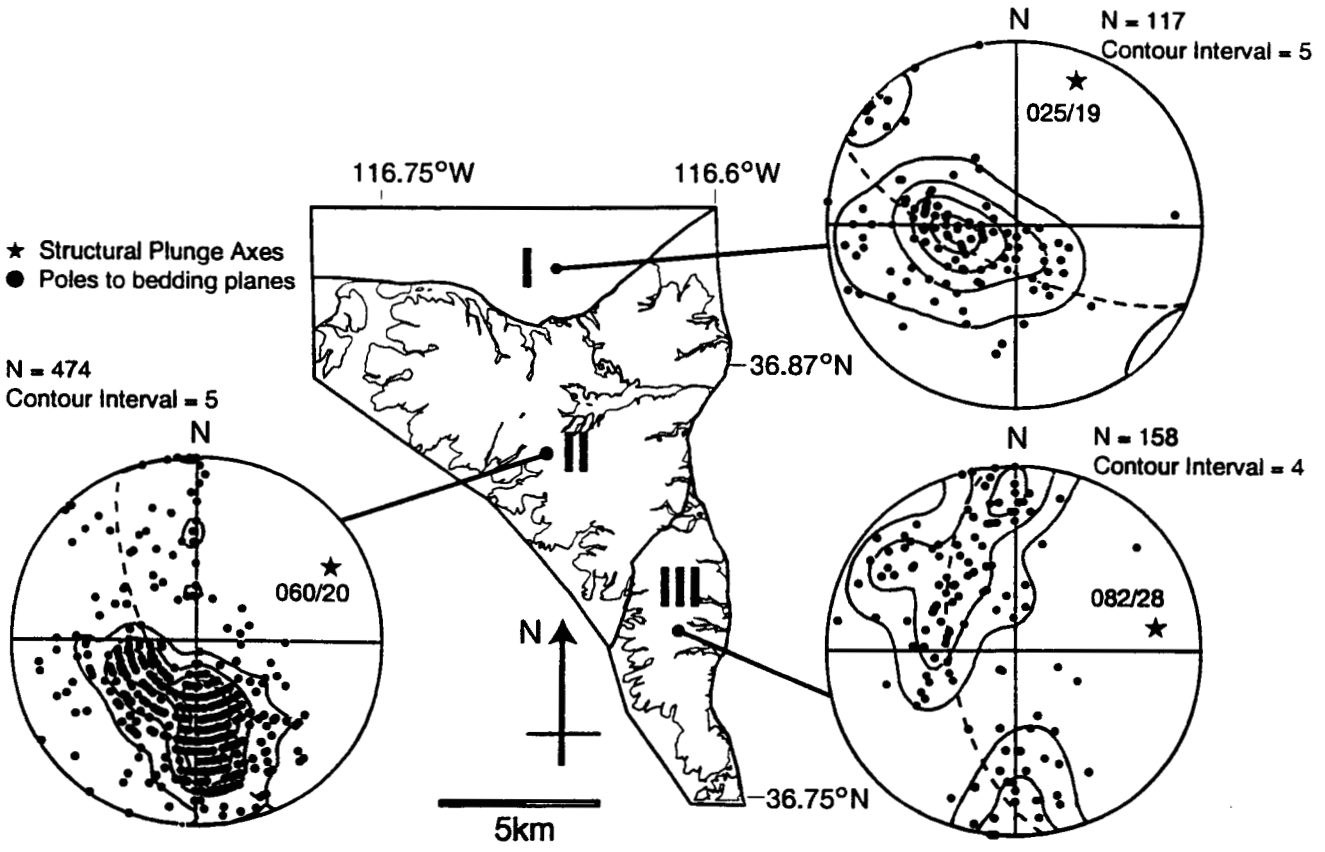

Figure 3
Ferrill et al.

311357 LH

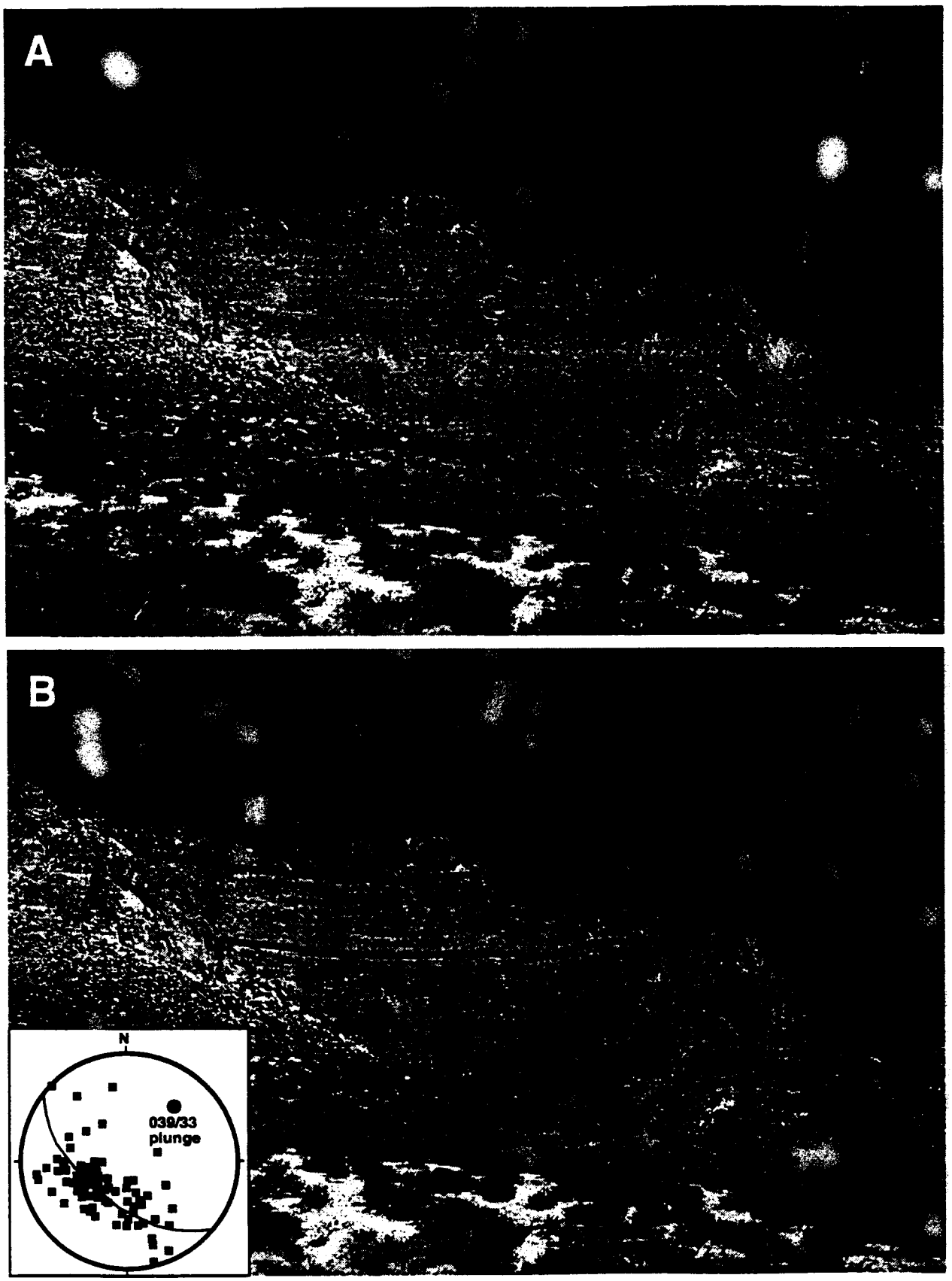

Ferrill et al.
Fig. 4

32/387 LH

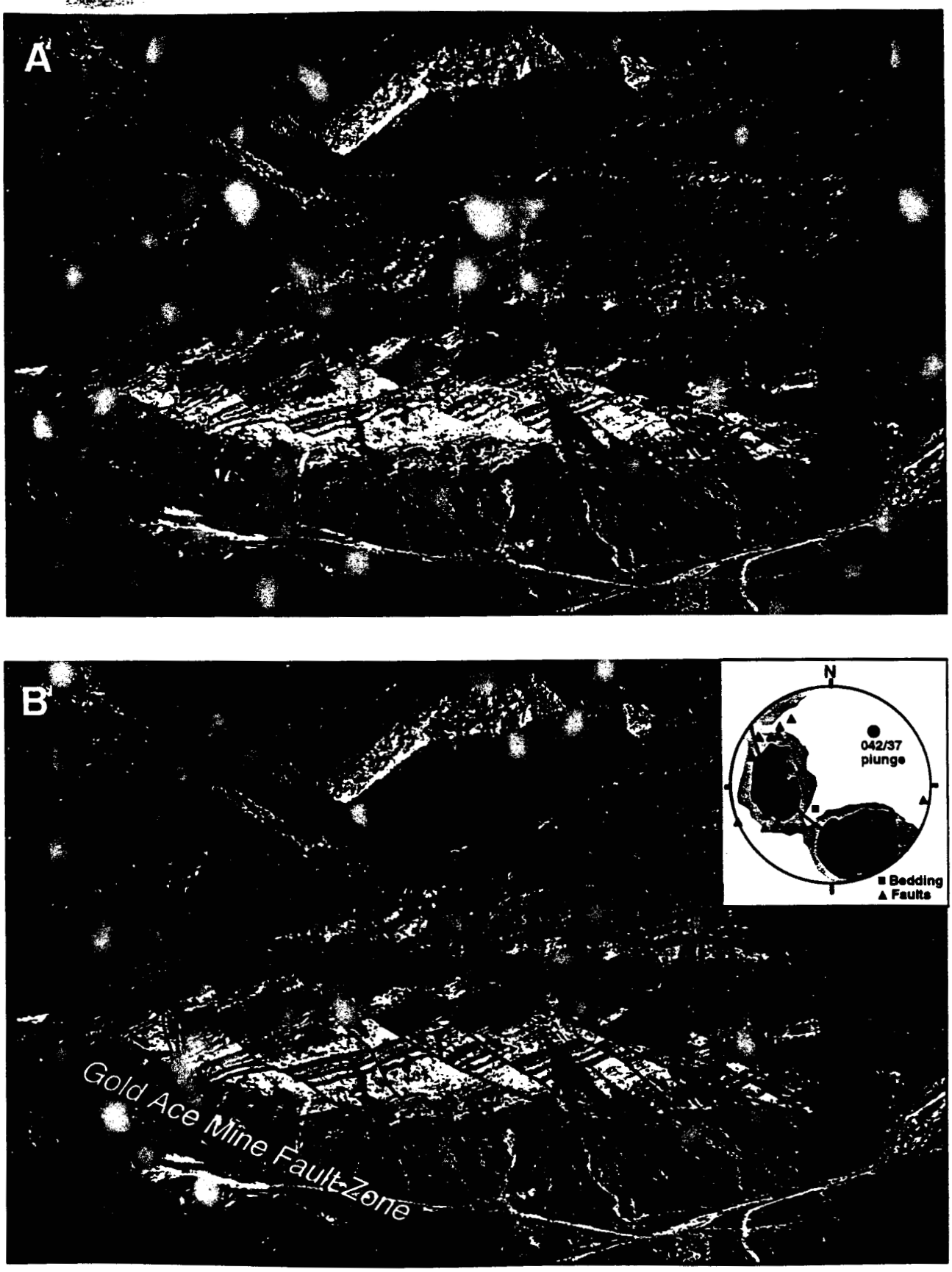

Ferrill et al.
Fig. 5

33/351
24

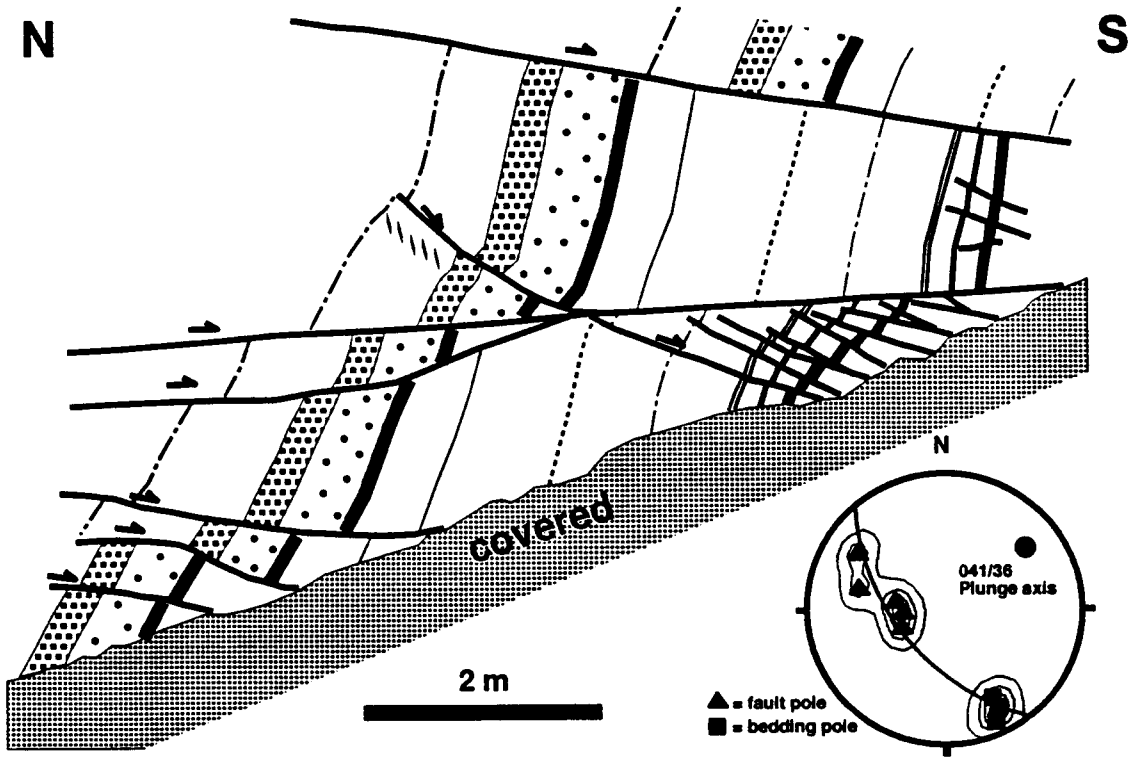

Ferrill et al.
Fig. 6

34/357
YA

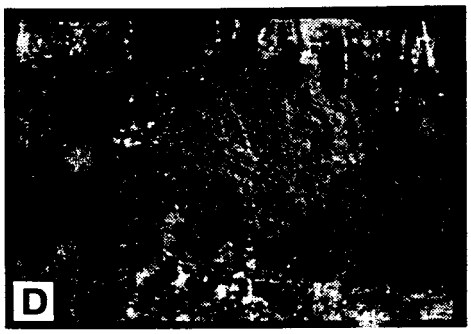

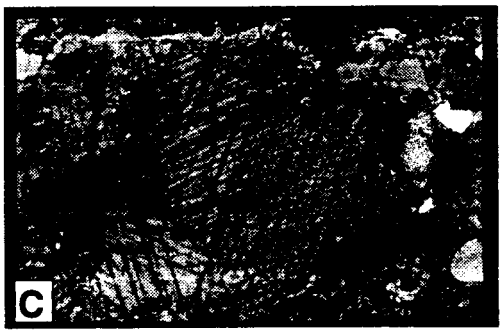

Photomicrograph scale

1 mm

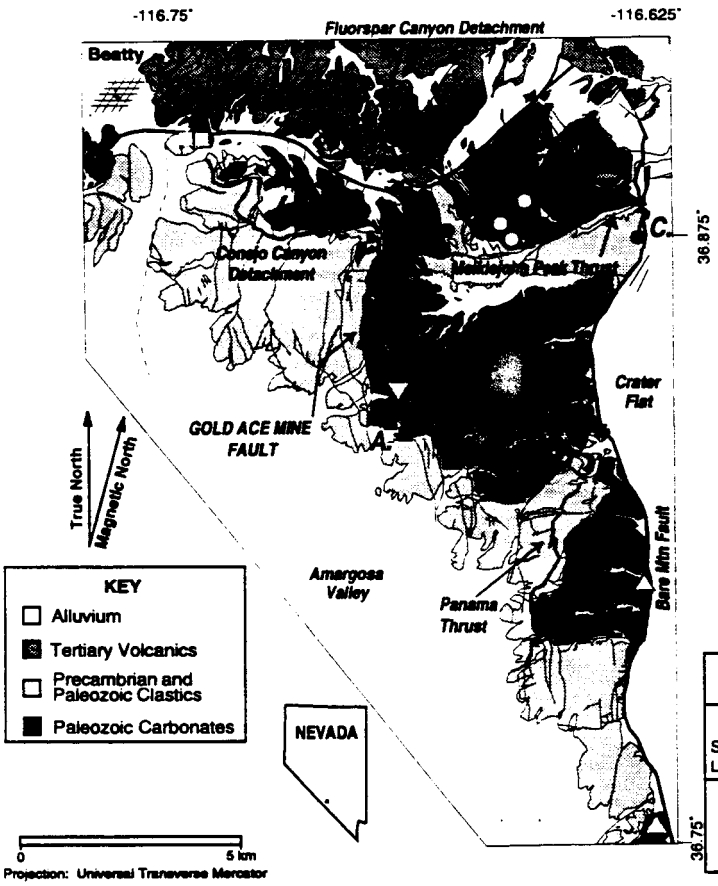

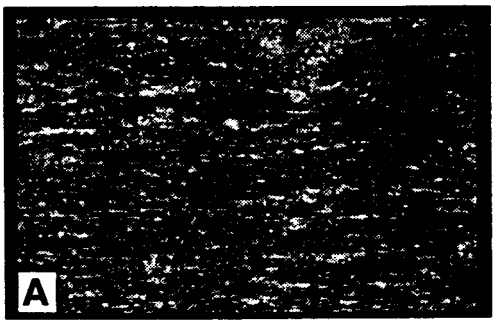

Key to Calcite Twin Sample Temperatures		
Sample Locations	Sample Locations used to calculate geotherm	Temperature
○	●	150°-200°C
△	▲	200°-300°C
▽	▼	>250°C
□	■	Recrystallization

Ferrill et al.
Fig. 7

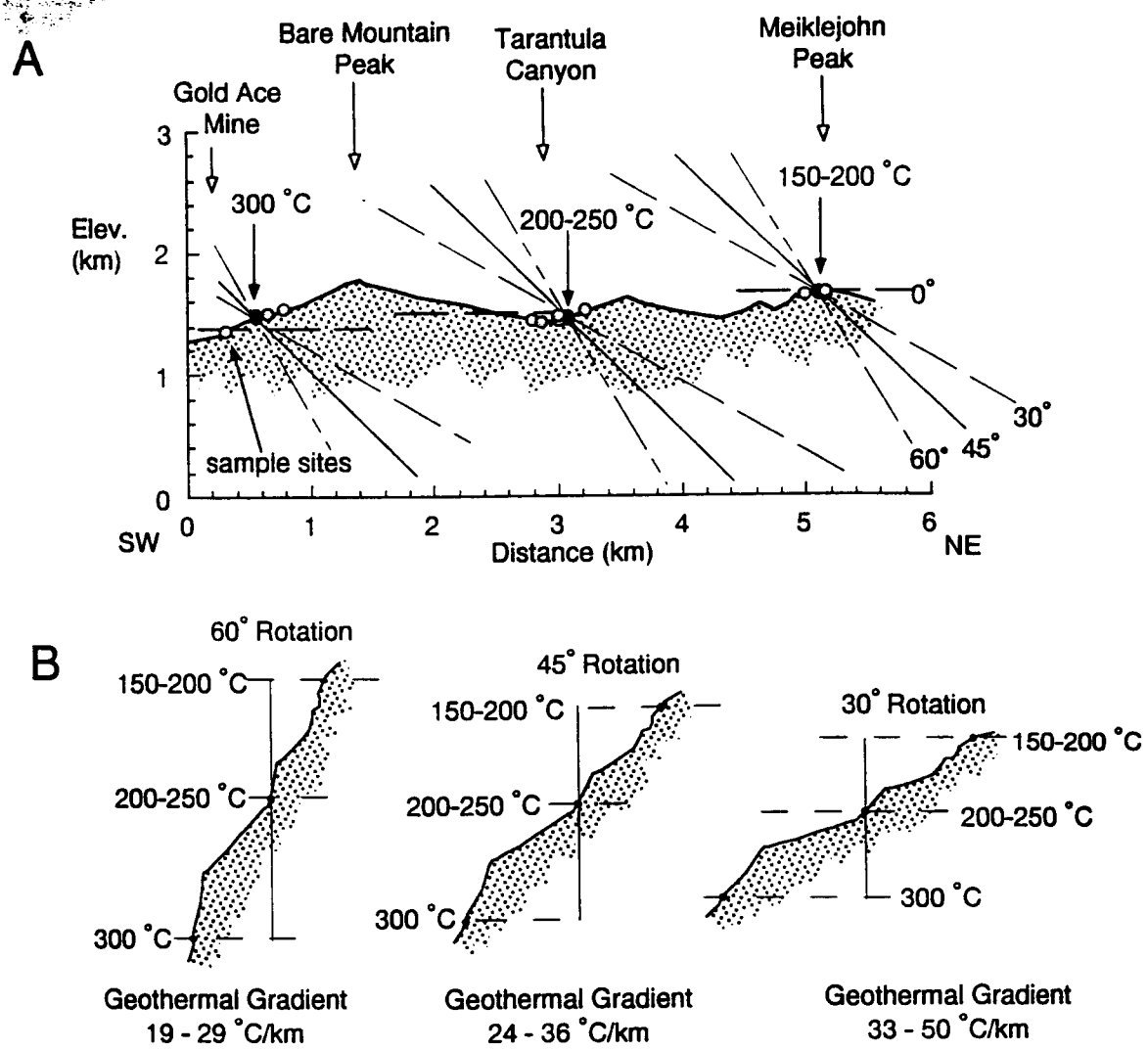

Ferrill et al.
Fig. 8

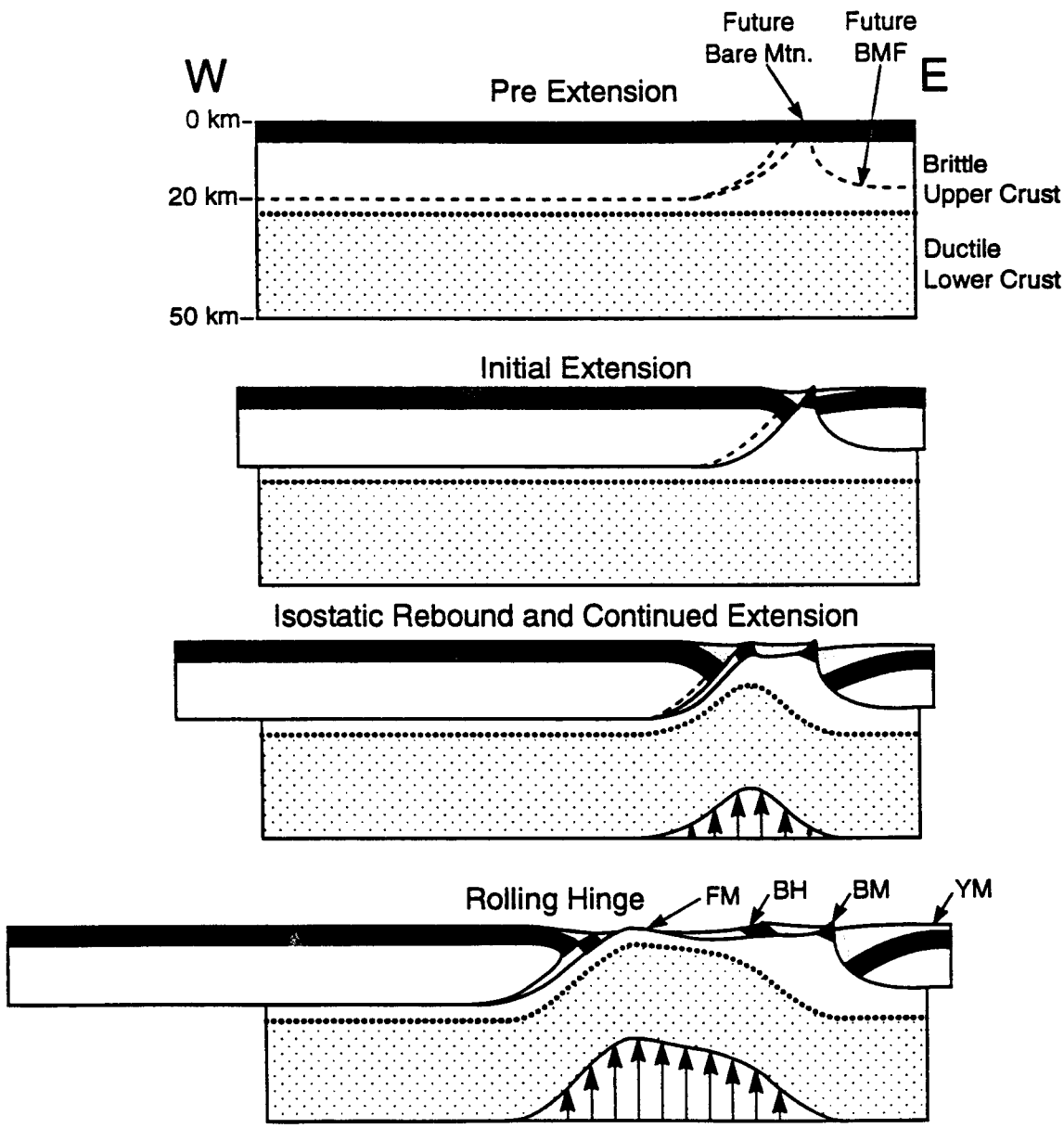

Ferrill et al.
Fig. 9

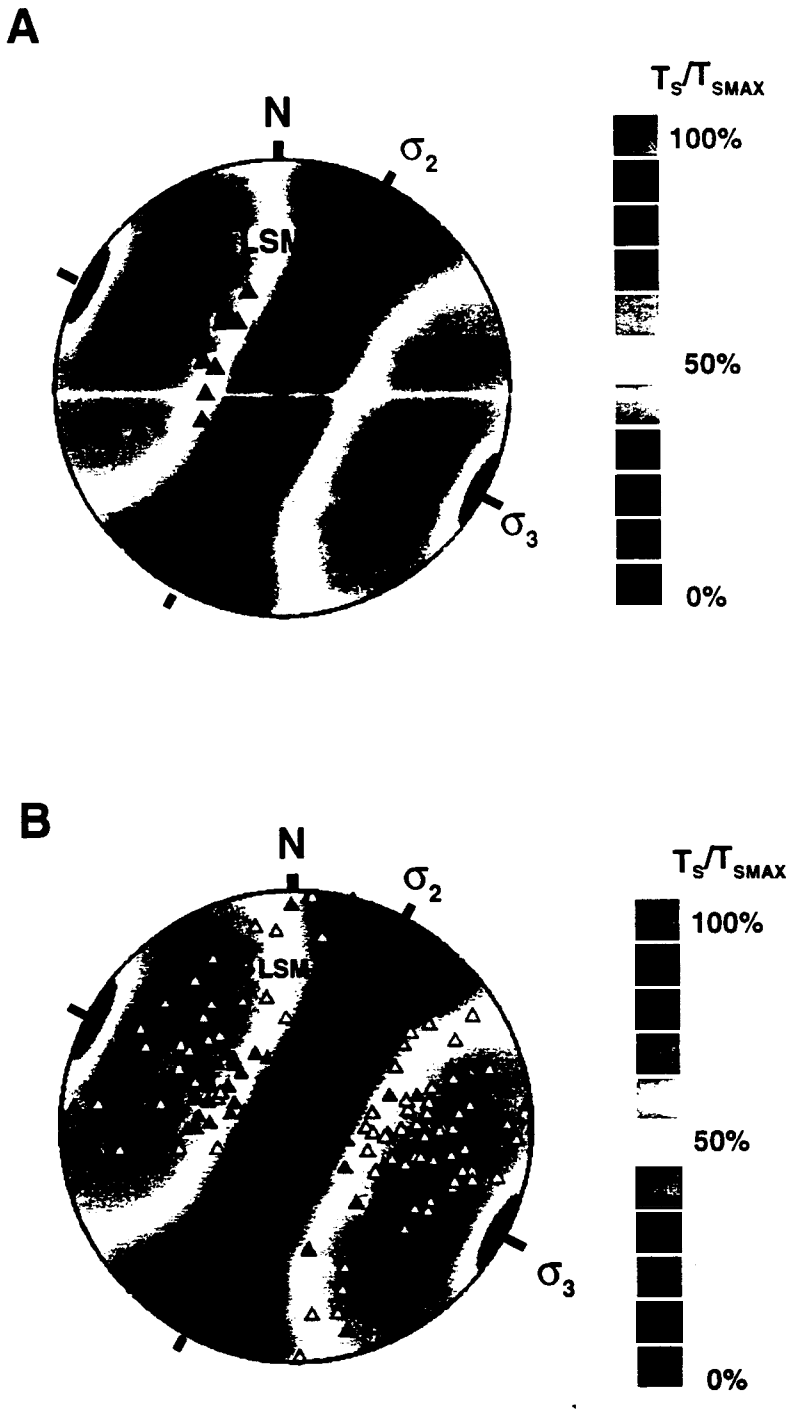

Ferrill et al.
Fig. 10